MDPI

Article

Evaluating MULTIOBS Chlorophyll-a with Ground-Truth Observations in the Eastern Mediterranean Sea

Eleni Livanou [1],*, Raphaëlle Sauzède [2], Stella Psarra [3], Manolis Mandalakis [4], Giorgio Dall'Olmo [5], Robert J. W. Brewin [6] and Dionysios E. Raitsos [1]

1 Department of Biology, National and Kapodistrian University of Athens, 15772 Athens, Greece; draitsos@biol.uoa.gr
2 Institut de la Mer de Villefranche, Sorbonne Université, CNRS, 06230 Villefranche-sur-Mer, France; raphaelle.sauzede@imev-mer.fr
3 Institute of Oceanography, Hellenic Centre for Marine Research, 71003 Heraklion, Greece; spsarra@hcmr.gr
4 Institute of Marine Biology, Biotechnology and Aquaculture, Hellenic Centre for Marine Research, 71003 Heraklion, Greece; mandalakis@hcmr.gr
5 National Institute of Oceanography and Applied Geophysics—OGS, Borgo Grotta Gigante 42/c, Sgonico, 34010 Trieste, Italy; gdallolmo@ogs.it
6 Centre for Geography and Environmental Science, Department of Earth and Environmental Sciences, Faculty of Environment, Science and Economy, University of Exeter, Cornwall TR10 9FE, UK; r.brewin@exeter.ac.uk
* Correspondence: eleniliva@biol.uoa.gr

Abstract: Satellite-derived observations of ocean colour provide continuous data on chlorophyll-a concentration (Chl-a) at global scales but are limited to the ocean's surface. So far, biogeochemical models have been the only means of generating continuous vertically resolved Chl-a profiles on a regular grid. MULTIOBS is a multi-observations oceanographic dataset that provides depth-resolved biological data based on merged satellite- and Argo-derived in situ hydrological data. This product is distributed by the European Union's Copernicus Marine Service and offers global multiyear, gridded Chl-a profiles within the ocean's productive zone at a weekly temporal resolution. MULTIOBS addresses the scarcity of observation-based vertically resolved Chl-a datasets, particularly in less sampled regions like the Eastern Mediterranean Sea (EMS). Here, we conduct an independent evaluation of the MULTIOBS dataset in the oligotrophic waters of the EMS using in situ Chl-a profiles. Our analysis shows that this product accurately and precisely retrieves Chl-a across depths, with a slight 1% overestimation and an observed 1.5-fold average deviation between in situ data and MULTIOBS estimates. The deep chlorophyll maximum (DCM) is adequately estimated by MULTIOBS both in terms of positioning (root mean square error, RMSE = 13 m) and in terms of Chl-a (RMSE = 0.09 mg m^{-3}). The product accurately reproduces the seasonal variability of Chl-a and it performs reasonably well in reflecting its interannual variability across various depths within the productive layer (0–120 m) of the EMS. We conclude that MULTIOBS is a valuable dataset providing vertically resolved Chl-a data, enabling a holistic understanding of euphotic zone-integrated Chl-a with an unprecedented spatiotemporal resolution spanning 25 years, which is essential for elucidating long-term trends and variability in oceanic primary productivity.

Keywords: chlorophyll-a; ocean colour remote sensing; phytoplankton vertical distribution; MULTIOBS; Argo floats; Eastern Mediterranean Sea

1. Introduction

The Eastern Mediterranean Sea (EMS) is an ultra-oligotrophic environment, experiencing a progressive warming trend over the last decades [1,2]. Climate model predictions identify the Mediterranean Sea as a climate change hotspot, where the warming trends and the frequency of extreme events are expected to intensify in the future [3,4]. Thus, the EMS may serve as a "laboratory" for what can be expected in other oceanic regions

under warmer climate scenarios [5,6]. Remotely sensed observations are the only available long-term dataset for chlorophyll-a concentration (Chl-a), a proxy for phytoplankton biomass and one of the essential ocean variables (EOVs) and essential climate variables (ECVs). However, these observations provide information only for the surface layer of the ocean, corresponding to the first optical depth, which sustains only up to one-fifth of the total Chl-a present within the entire euphotic zone [7]. Information about the vertical distribution of Chl-a in the EMS has been provided from in situ yearly monitoring studies conducted at fixed stations [8,9], oceanographic cruises [10,11], a limited number of BGC-Argo floats [12–14], modelling studies [15,16], and meta-analyses [17,18]. These studies conclude that Chl-a vertical distribution in the EMS can be highly variable and confirm the semi-permanent occurrence of a deep chlorophyll maximum (DCM) that is present from spring to autumn and typically located below 50 m. Nevertheless, our current understanding of Chl-a vertical distribution in the region is constrained by the limited spatial coverage of in situ and BGC-Argo observations. Furthermore, the EMS has been significantly under-sampled in terms of Chl-a, compared with the western part of the Mediterranean Sea. Despite some efforts to maintain time series data at selected EMS ocean observatories [9,19], long-term observations with adequate temporal resolution for climate-change studies are currently missing from this area, hindering progress in understanding the effects of climate change on phytoplankton communities. Modelling studies, on the other hand, are valuable in providing mechanistic insights into the biogeochemical functioning of marine ecosystems and in driving hypothesis formulation. However, their predictive capability remains constrained by our current understanding of oceanic biogeochemical and physical processes that can be represented mathematically in model structures.

The Multi Observations Thematic Assembly Center (MOB TAC) of the European Union's Copernicus Marine Service release a Global Ocean 3D Chl-a concentration product, which provides multiyear, global gridded fields of vertically resolved Chl-a profiles at a weekly temporal resolution. This product offers a unique platform for studying the spatiotemporal variability of the entire phytoplankton assemblage in relation to the physical variability of the water column, particularly under the immediate influence of climate change. Nevertheless, to date, this product remains relatively under-exploited by the scientific community. Despite the rigorous calibration and validation presented in the quality information document (QUID) of the product [20], its performance has only been evaluated against in situ high-performance liquid chromatography (HPLC) measurements of Chl-a roughly at a global scale. In this study, we use an independent dataset of in situ HPLC Chl-a data, collected during various oceanographic missions in the Levantine and Cretan Seas over a 14-year period (2008–2022), to assess the performance of the MULTIOBS Chl-a product in the ultra-oligotrophic environment of the EMS, both in terms of absolute Chl-a concentration and profile shape characteristics.

2. Methods

2.1. MULTIOBS Product

The global ocean 3D product MULTIOBS_GLO_BIO_BGC_3D_REP_015_010 [21] (hereafter called MULTIOBS) was acquired from the Copernicus Marine Service (Ramonville-Saint-Agne, France). This product provides a 3D global reconstruction at a 0.25-degree resolution for depth profiles of the particulate backscattering coefficient (b_{bp}) and its derived product (i.e., particulate organic carbon; POC) and total Chl-a with a weekly temporal resolution spanning from January 1998 to December 2022.

The product is based on a neural network method (multi-layer perceptron, MLP) developed by Sauzède et al. (2016) [22] called SOCA2016 (satellite ocean colour merged with Argo data to infer bio-optical properties to depth). This method uses as inputs satellite ocean colour bio-optical products (b_{bp} and Chl-a) matched with physical properties (i.e., specific density values and mixed layer depth (MLD)) derived from Argo temperature–salinity profiles and temporal information from the satellite–Argo matchups (i.e., day of

year) to estimate the vertical distribution of b_{bp}. The MLP is trained using as a reference the b_{bp} measured from Biogeochemical-Argo floats (BGC-Argo; [23]). Since its initial release, SOCA2016 has been upgraded to SOCA2024 to retrieve the b_{bp} and Chl-a profiles of the 3D gridded MULTIOBS product. Significant changes in the SOCA2024 method, compared with the SOCA2016 method, among others, include: (i) the addition of sea level anomaly (SLA), absolute dynamic topography (ADT), and photosynthetically available radiation (PAR) to the input parameters of the neural network; (ii) the replacement of Chl-a and b_{bp} inputs by the median (8 days and a micropixel of 5×5 pixels) of the remote sensing reflectance (R_{rs}) at five wavelengths for each matchup (and the addition of the standard deviation the R_{rs} at 412 nm); (iii) the replacement of the four Argo temperature–salinity-derived density values in the euphotic layer by principal component analysis (PCA) components for the entire temperature and salinity profiles; (iv) the inclusion of latitude and longitude in the input parameters; (v) improved accuracy of b_{bp} and Chl-a profiles training datathrough state-of-the-art processing in the delayed mode; and (vi) improved performance of the neural network by using an ensemble of the best MLPs, which also allowed for uncertainty quantification in the model estimates. Further details are given in the quality information document of the product [20].

The input physical parameters for the SOCA2024 used for the estimation of weekly bio-optical profiles (b_{bp}, and Chl-a) are derived from weekly temperature–salinity and MLD fields available from MULTIOBS_GLO_PHY_TSUV_3D_MYNRT_015_012 [24] at a $0.25° \times 0.25°$ spatial resolution. Input surface components for SOCA2024 correspond to the same period and are re-gridded to a $0.25° \times 0.25°$ spatial resolution, and these include: (i) medians (and standard deviation) of the daily reflectance fields obtained from the Copernicus Marine Service multi-sensor (SeaWiFS, MODIS-Aqua, MERIS, and VIIRS sensors) reprocessed product OCEANCOLOUR_GLO_BGC_L3_MY_009_103 [25], (ii) averages of the daily SLA and ADT fields from SEALEVEL_GLO_PHY_L4_MY_008_047 [26], and (iii) averages of the daily PAR fields available from the GlobColour website [27].

For this study, Chl-a vertical profiles within the 0–150 m depth layer were used. The depth resolution was 5 m within the 0–70 m layer, 10 m within the 70–100 m layer, and 25 m within the 100–150 m depth layer. Linear interpolation between these depths was performed to generate continuous vertical profiles of Chl-a.

2.2. In Situ HPLC Data of Chl-a

From the HPLC Chl-a database, maintained by the Hellenic Centre for Marine Research (HCMR), 86 in situ profiles that matched MULTIOBS data in both space and time in the EMS were selected (Figure 1). For temporal matchup, MULTIOBS data were selected from the nearest date to the in situ measurements. With regard to spatial matchup, the closest to the in situ, non-null MULTIOBS grid point from a 3-by-3 pixel box centered around the location of in situ data was used. These criteria resulted in an average (minimum–maximum) time and distance difference of 1 (−3, +3) day and 15 (2–42) km between MULTIOBS and in situ data. Overall, 39 profiles were matched to their exact grid point, whereas for the remaining 47 in situ Chl-a profiles, the closest non-null grid point from the 3-by-3 pixel box was selected.

The resulting HPLC Chl-a database consists of profiles collected during 7 oceanographic cruises within the frame of EU and national projects (SESAME-IP (2008), PERSEUS-IP (2013), KRIPIS I (2014–2015), LEVECO (2016), and JRC-SHIPSUPPORT I (2022)) and a time series data set collected from the POSEIDON E1-M3A buoy (WMO 61277), located 24 nautical miles north of Crete island (approx. 35.736°N, 25.122°E) at a depth of 1400 m [19]. To determine Chl-a by HPLC, 2 L of seawater were filtered through GF/F filters (ø 25 mm), and the filters were immediately frozen in liquid nitrogen and stored at −80 °C until further analysis at the HCMR facilities. Chl-a extraction and the chromatographic conditions during HPLC analysis are described in Lagaria et al. (2017) [28]. Samples from SESAME 2008 were analysed in the Laboratoire d'Océanographie de Villefranche—(LOV).
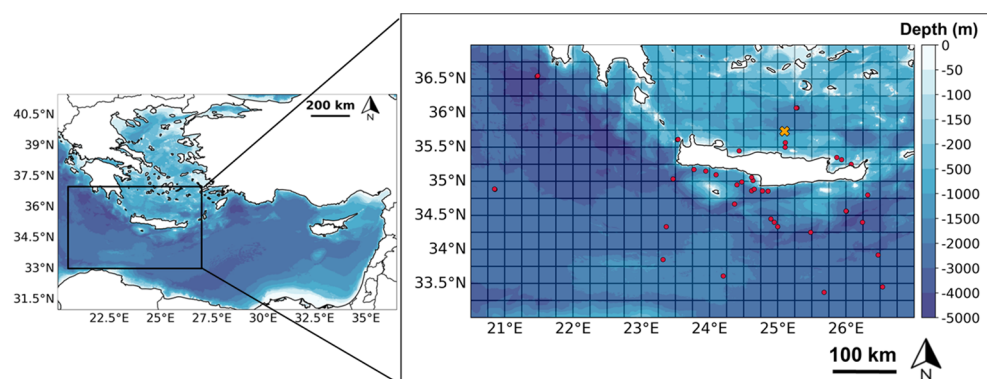
Figure 1. Locations of sampling stations for the available in situ data (red dots). The orange × symbol marks the position of the E1-M3A monitoring station. The grid lines represent the pixels of the MULTIOBS product. Bathymetry data were obtained from GEBCO_2021 grid dataset.

2.3. Data Processing and Analysis

The HPLC dataset consists of Chl-a measurements at 5–8 discrete depths across the euphotic zone (0–150 m). To minimise bias due to sampling at discrete depths, continuous vertical Chl-a profiles were calculated using the corresponding fluorescence profiles obtained from the CTD-mounted fluorometer that were calibrated with HPLC-derived Chl-a measurements using a linear model, following the methodology of Taillander et al. (2018) [29]. Out of the total 86 available HPLC Chl-a profiles, 80 had corresponding fluorescence profiles. The fluorescence profiles were treated to remove spikes according to D'Ortenzio et al. (2010) [30]. Possible non-photochemical quenching (NPQ) was accounted for following the procedure of Xing et al. (2012) [31], and the MLD needed for this correction was calculated according to the temperature criterion following de Boyer Montégut et al. (2004) [32]. To account for variations in the different sensors used during different cruises, HPLC measurements of Chl-a at discrete sampling depths were matched to the corresponding fluorescence values for each sampling occasion. Then, least squares linear regression between HPLC measurements and the corresponding NPQ-corrected and NPQ-uncorrected fluorescence profiles was used to derive the calibrated continuous fluorescence profiles. The coefficient of determination (r^2) associated with the linear regression was used as a criterion for selecting the most appropriate calibration method (corrected or uncorrected for NPQ) (Figures S1 and S2 in the Supplementary Materials). Only calibrated profiles with an $r^2 > 0.5$ were kept in the analysis. This criterion resulted in 74 calibrated fluorescence profiles out of the 80 that were paired with HPLC Chl-a profiles. The linear regressions produced an average r^2 of 0.89 (range: 0.51–0.99), with slopes ranging from 0.21 to 4.02 ($p < 0.05$) with an average value of 1.07 and intercepts ranging from −5.22 to 0.28 with an average value of −0.07. The wide range of slopes obtained during the calibration process agree with the well-documented variability of fluorescence-derived versus HPLC-derived Chl-a [31,33], which is highly dependent on the phytoplankton community composition at the time of sampling [34].

To maximise the in situ data available for comparison with the MULTIOBS product, the six profiles that did not have a good fit to the corresponding fluorescence profiles, probably due to the fluorescence probe malfunction, as well as the six profiles lacking any corresponding fluorescence profile, were linearly interpolated within their sampling depth range (0–120 m layer). This decision was supported by the adequate spread of samples from discrete depths across the 0–120 m layer, ensuring a good representation of the vertical Chl-a distribution irrespective of season (Figures S1 and S2). The common maximum depth for most of the in situ profiles, as well as the MULTIOBS profiles, was 120 m; thus, the 0–120 m layer was selected to form a uniform dataset.

The performance of MULTIOBS product in capturing the vertical variability of Chl-a was evaluated in terms of monthly climatologies, as well as in terms of one-to-one

comparisons via scatterplots between MULTIOBS-derived (linearly interpolated profiles) and in situ Chl-a (HPLC-calibrated fluorescence profiles) both for the whole water column and for various depth layers considered separately. For these comparisons, we used the matched in situ and MULTIOBS data at every 10 m interval within the 0–120 m depth layer. The one-to-one comparison was also performed for the HPLC bottle data and the matchups of MULTIOBS-derived Chl-a from the linearly interpolated profiles (Supplementary Materials). Additionally, the product's ability to reproduce DCM dynamics was evaluated by employing kernel density estimation plots with Gaussian kernels and boxplots. These plots were used to compare the distributions of the in situ- and MULTIOBS-derived positions of the DCM and of the Chl-a concentration at the DCM, calculated as the mean integral of a 20 m layer centred at the DCM. For this comparison, a subset of in situ and MULTIOBS matched-up profiles were selected, consisting of profiles exhibiting a DCM shape as defined by Lavigne et al., (2015) [17]. Time series plots were also generated to assess the ability of the product to capture the seasonal and interannual variability of integrated Chl-a within different depth layers. For this analysis, to minimise any spatial variability that could influence the results of this comparison, only the in situ data from the E1-M3A station were considered. The closest non-null pixel from the MULTIOBS product was selected (35.875°N, 25.125°E) (Figure 1). Integrations of Chl-a across successive depth layers were performed using the trapezoidal rule. Integrals were divided by the respective integration depth to calculate the mean Chl-a concentration for each sampling event and depth layer.

To quantify the MULTIOBS performance against in situ data, we used the Pearson's correlation coefficient (r) and corresponding significance (p) estimated by a two-sided *t*-test at a 0.05 significance level, along with the root mean square error (RMSE) Equation (1), representative of the precision of the product, and the bias Equation (2), representative of the accuracy of the product [35]. Chl-a data were $\log_{10}$-transformed for the statistical analysis to account for the log-normal distribution of these data [35],unless otherwise specified in the text. The evaluation of the calculated statistical metrics was based on back-transforming them from $\log_{10}$ space and then interpreting them as multiplicative factors [36].

$$RMSE = \sqrt{\frac{1}{n}\sum_{i=1}^{n}\left(X_i^M - X_i^O\right)^2} \tag{1}$$

$$bias = \frac{1}{n}\sum_{i=1}^{n}\left(X_i^M - X_i^O\right) \tag{2}$$

Additionally, the slope of the linear regression and the coefficient of determination (r^2) were calculated for $\log_{10}$-transformed Chl-a data, while the mean absolute percent difference (MAPD) Equation (3) and RMSE were also computed in the linear space to compare our results with those reported in the quality information document of the product [20].

$$MAPD = 100\% \times \frac{1}{n}\sum_{i=1}^{n}\left|\frac{X_i^O - X_i^M}{X_i^O}\right| \tag{3}$$

In Equations (1)–(3), X denotes Chl-a, and the superscripts O and M denote the observed in situ Chl-a and estimated Chl-a derived from MULTIOBS, respectively.

2.4. Software

Data visualisation and analysis were performed using Python3.12.2. Linear interpolations were performed with *scipy.interpolate*, integrations were carried out with *scipy.integrate*, Pearson's r was calculated using *scipy.stats* (scipy 1.12.0) [37], and ordinary least squares linear regressions were performed with *statsmodels* 0.14.0 [38]. Kernel density estimate plots and boxplots were constructed using the *seaborn* 0.12.2 library [39]. Data analysis was conducted using *pandas* 2.2.1 [40] and *xarray* 2023.6.0 [41]. Data visualisation was

performed using *matplotlib* 3.8.3 [42], and *cartopy* 0.22.0 [43] was also used to generate the map in Figure 1.

3. Results and Discussion

In this section, an in-depth evaluation of the MULTIOBS product performance in capturing various aspects of the variability and temporal dynamics of Chl-a vertical profiles in the EMS is presented, along with a discussion of the potential research applications of this new product.

3.1. Climatological Trends

The average monthly vertical Chl-a profiles obtained from in situ data in the EMS region, along with the corresponding matched (in space and time) vertical profiles from the MULTIOBS product, allow for a visual comparison of the in situ and estimated profile shapes throughout the seasonal cycle (Figure 2). The in situ climatological profiles are consistent with the typical Levantine basin patterns, which are characterised by generally low Chl-a (<0.25 mg m^{-3}). From December to March, increased surface Chl-a compared with deeper layers is observed. Additionally, the DCM occurs from April to November, migrating from its shallowest climatological depth of ~80 m during April to its deepest point (~100 m) in July and gradually resurfacing again to ~80 m towards winter. The product adequately reproduces the shape of the profiles and captures the progressive transition of the vertical Chl-a pattern, from a sigmoidal shape during the mixing period (January–February) to a gaussian shape, with the gradual establishment and deepening of the DCM from spring to autumn, followed by the erosion of the DCM with the onset of the next mixing period (November–December).
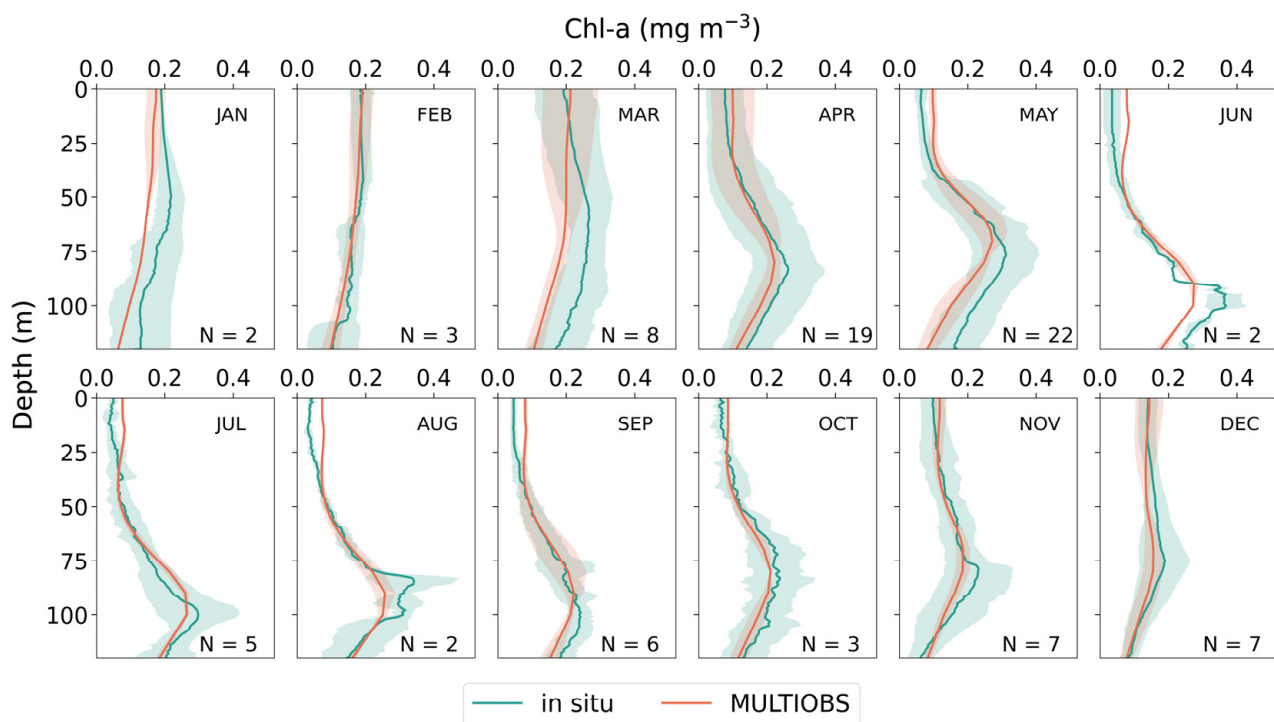
Figure 2. Monthly averaged vertical chlorophyll-a concentration (Chl-a) profiles obtained from in situ data over the Eastern Mediterranean Sea and the corresponding matched (in space and time) monthly averaged vertical profiles obtained from the MULTIOBS product. N denotes the number of matched profiles per month.

The highest (in absolute Chl-a values) inconsistencies between MULTIOBS and in situ data are observed in March at depths below 20 m (Figure 2 and Figure S3, Supplementary

Materials). During this month, in situ data suggest enhanced Chl-a, throughout the water column, with significant spatiotemporal variability. In contrast, the MULTIOBS product predicts substantial variability in the upper 60 m of the water column, whereas in the deeper layers, the product indicates a consistent reduction in Chl-a with increasing depth, accompanied by low variability. The in situ data presented here are distributed in a non-bloom region, according to the classification proposed by D'Ortenzio and Ribera d' Alcala (2009) [44] for the trophic regimes of the Mediterranean Sea. In these areas, surface Chl-a peaks during February–March and coincides with the annual maximum MLD [45]. Interannual and spatial variations in the MLD strongly influence the shape and concentration of Chl-a vertical profiles during the productive period. The EMS, including the South Aegean Sea, is characterised by a complex hydrological regime dominated by permanent and transient sub-mesoscale and mesoscale eddies [46,47]. These features can influence stratification and, consequently, MLD through vertical displacement of isopycnals, resulting in Chl-a patchiness [48]. Among the input parameters of the MLP employed to produce the MULTIOBS product, SLA represents mesoscale processes that influence the vertical distribution of phytoplankton biomass; ADT combines the variable component (i.e., SLA) with the stationary component of ocean circulation, thus providing information about large-scale ocean dynamics; and PAR is one of the main limiting factors for phytoplankton growth that directly affects Chl-a vertical distribution. The combination of these three parameters potentially allows for improved predictions of Chl-a vertical distribution in areas with complex hydrological regimes like the EMS. However, the discrepancies between in situ and MULTIOBS data, observed during March, may be explained by the relatively coarse spatiotemporal resolution (~25 km and weekly) of the product, as well as the extent of the grid used for the matchups (3-by-3 pixels), implying that these differences may simply be an artefact of the contrasting scales of the in situ and MULTIOBS data. A higher-resolution MULTIOBS product might result in better agreement with the in situ data during the period of the annual maximum (March). Finally, a systematic underestimation of Chl-a by the MULTIOBS product is evident in the vicinity of the DCM layer during the stratified period (May–September), especially at its onset (May–June). Conversely, during this same period, a systematic overestimation is observed in the upper 40 m of the water column. The reasons for these discrepancies are discussed in the next subsections.

3.2. Statistical Evaluation of MULTIOBS Data

The scatterplot for the matchups of in situ versus MULTIOBS Chl-a at every 10 m interval within the 0–120 m depth layer is shown in Figure 3a. The results show strong agreement between the two datasets (r = 0.77, $p < 0.001$), with most data points aligning closely with the 1:1 line. The bias reveals that the MULTIOBS product accurately estimates in situ data, with only a slight 1% overestimation. The RMSE suggests a 1.5-fold average deviation between in situ data and MULTIOBS estimates. However, MULTIOBS notably overestimates in situ Chl-a at the lower end of the concentrations range (0.01–0.05 mg m^{-3}) across the entire water column in the EMS (Figure 3a and residual plots shown in Figures S4a and S5a in the Supplementary Materials).

To gain a better understanding of how depth affects the performance of the MULTIOBS product against in situ data, we created additional scatterplots for three depth layers, and relevant statistical metrics were calculated and examined separately (Figure 3b–d). These layers were chosen to represent key zones of vertical Chl-a variability based on the climatological profiles (Figure 2). The surface–subsurface layer (0–50 m) exhibits a relatively homogenous distribution of Chl-a, the intermediate layer (60–100 m) encompasses the depths where the DCM is formed under non-mixed conditions, and the deepest layer in our dataset (110–120 m) corresponds to where Chl-a monotonically decreases with increasing depth.
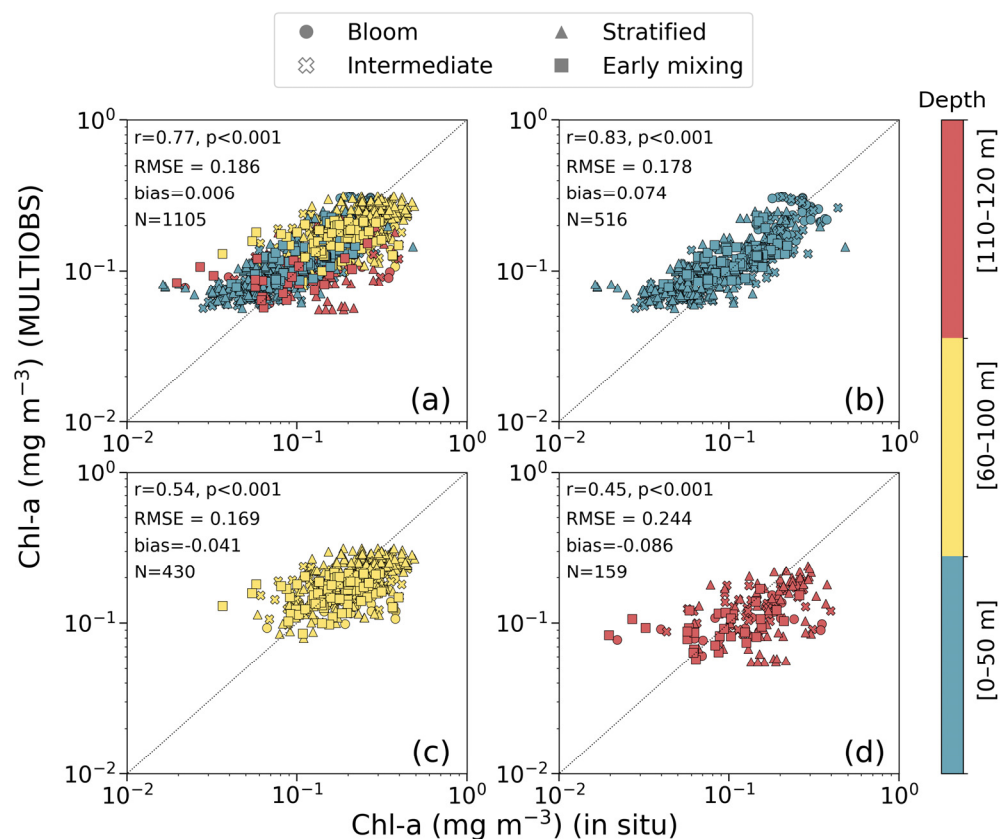
Figure 3. Scatterplots of the matchups between in situ- and MULTIOBS-derived chlorophyll-a concentration (Chl-a) over the Eastern Mediterranean Sea, with colours indicating the different depth layers. (**a**) Overall relationship across all depths within the 0–120 m layer, (**b**) surface layer scatterplot considering matchups within 0 to 50 m of depth, (**c**) intermediate layer scatterplot considering matchups within 60 to 100 m of depth, and (**d**) deeper layer relationship considering matchups within 110 to 120 m of depth. For clarity, only values at every 10 m interval within the 0–120 m depth layer are plotted. Different symbols represent distinct time periods: bloom [circle]—January–March; intermediate [× symbol]—April; stratified [triangle]—May–September; and early mixing [square]—October–December. The 1:1 line is shown as a black dotted line. Statistical metrics for MULTIOBS performance are provided in each panel (see Section 2 for abbreviations of metrics).

The correlation is strong and significant (r = 0.83, *p* < 0.001) within the upper 50 m of the water column, and data points are well distributed along the 1:1 line, suggesting that the MULTIOBS generally co-varies with the in situ data (Figure 3b). Within this layer, the MULTIOBS product overestimates in situ Chl-a concentration by 19% on average (Figure 3b), as is evident from the higher bias, than the one observed when considering the overall relationship (Figure 3a). The overestimation is more pronounced for a distinct cluster representing data points at the lower end of the Chl-a range (0.01–0.05 mg m^{-3}), within the 0–50 m layer of the EMS during the stratified period (May–September) (Figures 2, S4b and S5b). These discrepancies could be related to the phenomenon of the non-photochemical quenching (NPQ) correction method. NPQ is a mechanism resulting in reduced Chl-a fluorescence, and it is used by photosynthetic organisms to protect their light-harvesting apparatus from super-saturating light conditions [49]. NPQ is a well-known and challenging-to-resolve issue when estimating Chl-a profiles from fluorescence measurements. Although a correction for NPQ was applied to BGC-Argo Chl-a profiles used for the training and validation of the MLP employed to produce the MULTIOBS product using state-of-the-art procedures [50,51], finding a universally optimal correction approach for all oceanic regions remains a challenge [52]. In the future, improving the NPQ correction algorithms for fluorescence profiles may further enhance MULTIOBS estimates for the surface layer of the EMS.

In the deeper layers (60–100 m and 110–120 m), a notable drop in correlation strength is observed, although the correlation remains significant ($p < 0.001$), suggesting that the MULTIOBS product does not have a consistent, monotonous relationship with the in situ data within these layers (Figure 3c,d). The overestimation of Chl-a concentrations by the MULTIOBS product decreases from the surface (0–50 m) (Figure 3b) to the intermediate (60–100 m) (Figure 3c) and deeper layers (110–120 m) (Figure 3d), where the product underestimates the in situ data by 9 and 18%, respectively. In addition, the RMSE in the intermediate layer (Figure 3c) is comparable with that in the surface layer (Figure 3b) and the overall dataset (Figure 3a), suggesting similar levels of precision. However, the RMSE shows a substantial increase in the deepest layer, where a 1.8-fold average deviation between in situ data and MULTIOBS estimates is observed (Figure 3d).

A notable deviation from the 1:1 line is evident for data points representing the deeper layers (60–120 m), encompassing measurements in the upper end of Chl-a concentration range (>0.3 mg m^{-3}) (Figures 3c,d, S4c,d and S5c,d). These deviating data points, which signify an underestimation of in situ Chl-a by MULTIOBS, are associated either with the DCM layer during the intermediate, stratified, and early mixing periods or with the blooming season, especially during March (see also Figure 2). This indicates the presence of elevated Chl-a in the deeper layers of the euphotic zone, a feature that is not well captured by the MULTIOBS product. In contrast, an overestimation by the product is also evident within these deeper layers on a few occasions, especially during the early mixing period for very low in situ Chl-a (<0.05 mg m^{-3}) (Figures 3c,d, S4c,d and S5c,d). A possible explanation for the observed discrepancies could be the low vertical resolution of the product within the deeper layers of the productive zone (i.e., 10 m within the 70–100 m layer and 25 m within the 100–150 m layer). Finally, scatterplots showing only the HPLC bottle data at the sampling depths and the matchups of MULTIOBS-derived Chl-a provided in the Supplementary Materials (Figure S6) agree with the aforementioned results.

The slope and coefficient of determination (r^2) estimated in the current study imply a slightly lower performance for MULTIOBS compared with the results reported in the QUID of the product (Table 8 for the EMS in Sauzède et al. (2024) [20]) (Table 1). Moreover, the MAPD (36%) and the RMSE (0.07 mg m^{-3}) are higher than what was reported in the QUID [20] for the EMS (23% and 0.03 mg m^{-3}, respectively), suggesting a lower accuracy and precision of the MULTIOBS product as quantified by using the present in situ HPLC-derived Chl-a dataset as reference (Table 1). It is important to note that the training of the MLP used to produce MULTIOBS as well as the EMS-specific assessment of the MULTIOBS product conducted in the QUID [20] was based on BGC-Argo Chl-a, derived from fluorescence measurements, rather than HPLC-measured Chl-a. The Mediterranean Sea is well represented in the BGC-Argo database used to train SOCA2024, with approximately 6000 profiles, including around 3500 in the EMS. Although MULTIOBS is not a regional product, this strong representation in the method that this product relies on contributes to its expected high performance in the Mediterranean region. However, there is a well-documented variability in the relationship between fluorescence signal and the "true" Chl-a due to variations in the physiological state of the cells as well as the taxonomic composition of phytoplankton assemblage [33,34]. These variations in Chl-a concentration versus fluorescence signal may explain the lower performance of the product documented in the present study using HPLC-measured Chl-a as reference data. On the other hand, the standardised metrics MAPD (36%) and r^2 (0.59) calculated in this study using the HPLC-based Chl-a dataset from the EMS suggests a better performance of the product when considering the corresponding metrics reported in the QUID [20] for the HPLC-assessed Chl-a global dataset (40% and 0.53, respectively) (Table 1). Finally, it is also worth stressing that the use of daily in situ data in this study, compared with the weekly temporal resolution of the MULTIOBS product, is a potential source of uncertainty that could influence the performance evaluation of the product. The coarse spatial resolution of the product may also contribute to uncertainties in the matchups.

Table 1. Statistical metrics calculated in this study, considering all depths (Figure 3a), compared with those provided in the quality information document (QUID) of the product (Table 8 and Figure 18; [20]). Note that, to be comparable with the QUID, root mean square error (RMSE) and mean absolute percent difference (MAPD) are calculated here in the linear space.

Dataset	Study	Area	r^2	Slope	RMSE (mg m^{-3})	MAPD (%)
HPLC	This study	EMS	0.59	0.51	0.07	36
BGC-Argo	QUID	EMS	0.83	0.81	0.03	23
HPLC	QUID	Global	0.53	0.70	0.34	40

3.3. Evaluation of Deep Chlorophyll Maximum Location and Magnitude Estimates

The DCM corresponds to a pronounced peak in the Chl-a distribution that is formed under stratified conditions [53]. In the EMS, DCM is present from April to November [17] and constitutes an important feature of the vertical Chl-a distribution. The DCM can either be associated with actual carbon biomass accumulation and significant primary production [54,55] or it can result from enhanced cellular chlorophyll-a content due to photoacclimation of phytoplankton cells to optimise growth at suboptimal light intensities, without a corresponding increase in their carbon biomass [12,56–59]. Therefore, capturing and understanding DCM dynamics is crucial to accurately assess aquatic primary production [60–62]. For this reason, here, we also assessed the ability of the MULTIOBS product to reproduce important DCM features i.e., its depth and its magnitude. These traits convey information about the shape of the Chl-a profile [17,63] that, in conjunction with environmental (e.g., light and nutrients availability) and/or biological variables (e.g., b_{bp} coefficient profiles), may advance our understanding of phytoplankton ecology in the lower part of the euphotic zone [14,56,64].

The calculation of relevant statistical metrics for the estimation of the DCM position and magnitude was performed in linear space, as data distributions were approximately normal (Figure 4). Results suggest a strong and significant correlation (r = 0.65, *p* < 0.001, N = 65) between the depth of the DCM derived from in situ data and the corresponding estimate from the MULTIOBS product. The DCM is accurately estimated by the MULTIOBS product, with the average bias being only −4 m, while the precision, indicated by the RMSE being calculated at 13 m is acceptable, considering the 5–10 m vertical resolution of the MULTIOBS product within the 50–100 m layer, where the DCM is mostly formed. Moreover, as shown in Figure 4a, the distribution of MULTIOBS-derived DCM depth is slightly skewed towards shallower depths, with 100 m being the deepest estimated position of the DCM (range: 50–100 m). On the other hand, in situ data show a more symmetrical distribution of DCM positions around the mean DCM depth of 84 m, with roughly equal representation of shallower and deeper DCMs (DCM range: 46–120 m).

Regarding Chl-a at the DCM, the correlation between the MULTIOBS and the in situ data is significant, albeit moderate (r = 0.32, *p* = 0.01, N = 65). The MULTIOBS product underestimates the DCM Chl-a by 0.053 mg m^{-3} on average, and the RMSE suggests an average deviation of 0.090 mg m^{-3} between MULTIOBS and in situ values at the DCM level. When comparing the distributions of MULTIOBS and in situ Chl-a concentrations at the DCM (Figure 4b), it is obvious that MULTIOBS predicts a somewhat narrower range of Chl-a concentrations at the DCM (0.153–0.303 mg m^{-3}) compared with the slightly wider range observed in situ (0.115–0.461 mg m^{-3}). It is worth noting that an important fraction of the inherent variation of in situ data at the DCM level might not be captured by MULTIOBS due to the coarse vertical resolution of the product, which is at 10 m within the 70–100 m layer, where DCM is mostly found.
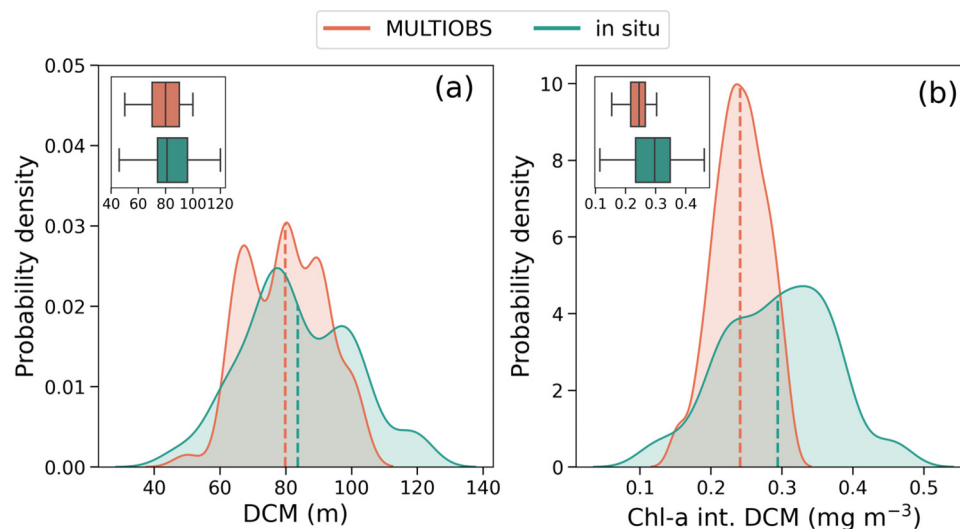
Figure 4. Distribution of in situ and MULTIOBS data derived for the Eastern Mediterranean Sea, showing (**a**) the position of deep chlorophyll maximum (DCM) and (**b**) the chlorophyll-a concentration (Chl-a) at the DCM, calculated as the mean integral of a 20 m layer centred at the DCM. Data are presented using kernel density estimation plots with boxplots shown as insets. Only matched-up profiles characterised as DCM type are analysed. Dashed line represents the mean of each distribution.

3.4. Seasonal and Interannual Variability

Long-term continuous phytoplankton time series convey ecological information about the changes occurring in phytoplankton assemblage over extended periods of time, playing a crucial role in understanding and monitoring the dynamics of marine systems [65]. These datasets allow researchers to detect trends and identify patterns of phytoplankton indicators like Chl-a (a proxy of phytoplankton biomass), phytoplankton community structure, as well as phenology metrics such as the timing of phytoplankton bloom initiation, maximum amplitude, termination, and duration [66]. Thus, phytoplankton time series can be used to assess the impact of climate change [67], interannual variability of physical forcing, nutrient availability [68], and extreme events [69,70] on phytoplankton indicators and, therefore, on oceanic production and carbon cycling. To date, most studies on these topics have employed ocean colour remote-sensing observations, as they meet the criteria for conducting this analysis (i.e., long-term, with adequate spatiotemporal coverage) [71,72]. However, remote-sensing data are limited to the surface layer of the ocean, specifically corresponding to the first optical depth. This limitation is significant when analysing oceanic processes that extend beyond this upper layer. Thus, the MULTIOBS product offers a notable advantage for time series studies that require detailed biomass information in deeper layers. The product meets the key requirements of continuous recordings with sufficient spatial and temporal resolution, essential for understanding long-term trends and variability. Additionally, MULTIOBS provides observations that encompass the entire euphotic zone, making it especially useful for comprehensive studies of the ocean's biologically productive zone. Consequently, here, we focus on evaluating the performance of the MULTIOBS product in providing information on the interannual variability of the phytoplankton biomass throughout the water column.

To assess the ability of the MULTIOBS product to capture the seasonal and interannual variability of Chl-a, we selected a subset of the dataset that included only the data from the E1-M3A monitoring site in the Cretan Sea (Figure 1). Time series of in situ versus MULTIOBS Chl-a, presented as the mean integrals within successive depth layers as well as for the entire euphotic zone (0–120 m), are shown in Figures 5 and 6, respectively, along with relevant statistical metrics. To further assess the ability of MULTIOBS to capture the seasonal variability within the successive depth layers at E1-M3A site, we also compare the average monthly climatologies of the matched-up in situ and MULTIOBS data (Figure S7). Additionally, scatterplots of the

monthly standardised anomalies of these matchups, calculated based on the aforementioned climatologies, are used to further assess the ability of the MULTIOBS to capture the interannual variability within the different depth layers at the E1-M3A site (Figure S8).
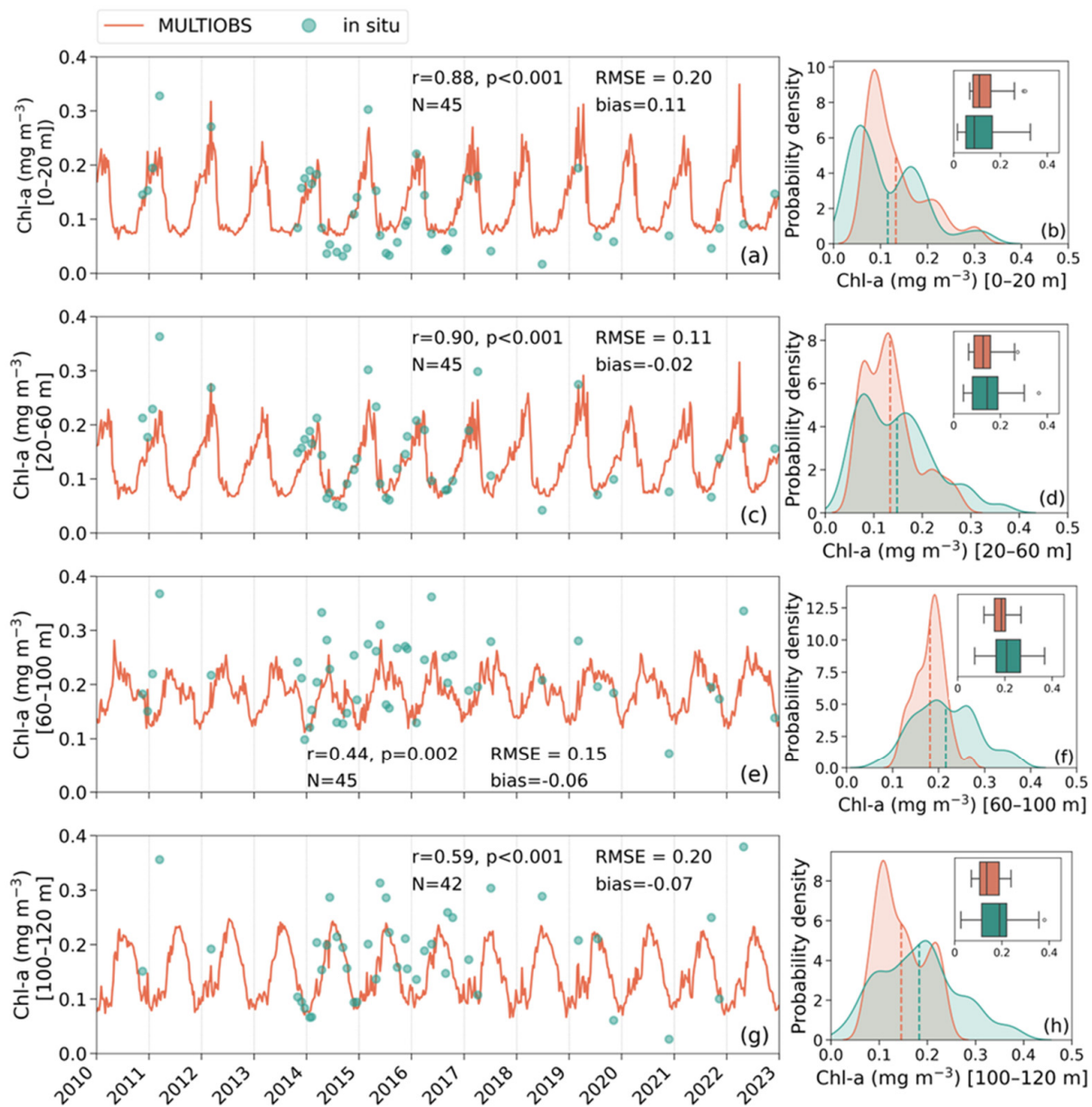
Figure 5. Time series of chlorophyll-a concentration (Chl-a) at the E1-M3A site at the Eastern Mediterranean Sea (north of Crete), derived from the in situ data (circles) and from the MULTIOBS data (line), presented as mean integrals of successive depth layers: (**a**) (0–20 m), (**c**) (20–60 m), (**e**) (60–100 m), and (**g**) (100–120 m). Statistical metrics are calculated for the $\log_{10}$-transformed data (see Section 2 for abbreviations of metrics). N indicates the number of observations per depth layer. The corresponding distributions of Chl-a at the E1-M3A site derived from the in situ data and their matchups from MULTIOBS data are summarised using kernel density estimation plots of the distributions of in situ- and MULTIOBS-derived Chl-a mean integrals of successive depth layers: (**b**) (0–20 m), (**d**) (20–60 m), (**f**) (60–100 m), and (**h**) (100–120 m). The dashed line indicates the mean of each distribution.
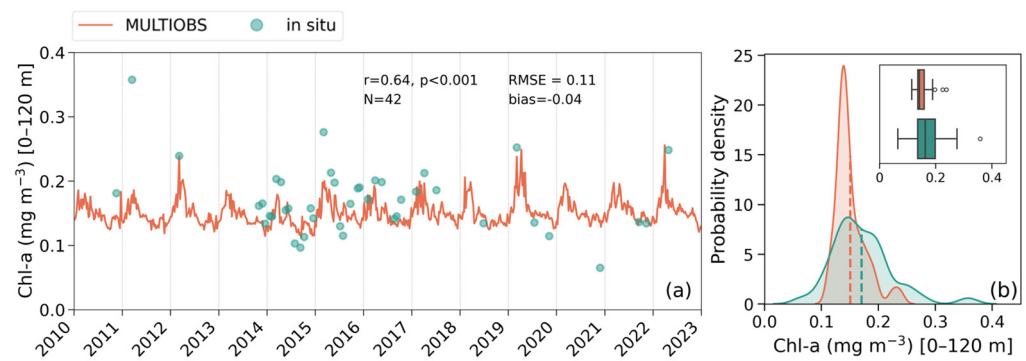
Figure 6. (**a**) Time series of chlorophyll-a concentration (Chl-a) at the E1-M3A site at the Eastern Mediterranean Sea (north of Crete) derived from the in situ data (dots, N = 42 profiles) and from the MULTIOBS data (line), presented as mean integrals of the 0–120 m layer. Statistical metrics are calculated for the $\log_{10}$-transformed data (see Section 2 for abbreviations of metrics). (**b**) Distributions of Chl-a at the E1-M3A site derived from the in situ data and their corresponding estimates from MULTIOBS (N = 42 profiles). Data are summarised using kernel density estimation plots of the distributions of in situ- and MULTIOBS-derived Chl-a presented as mean integrals of the 0–120 m layer. The dashed line indicates the mean of each distribution.

An excellent agreement between in situ and MULTIOBS data is observed within the upper (0–20 and 20–60 m) layers of the water column (Figure 5a–d). For example, in situ data show that the annual maxima of 2012, 2015, 2017, and 2019 were substantially higher than the annual maxima of 2014 and 2016, a pattern that is reproduced by the MULTIOBS both qualitatively as well as quantitatively. The correlation between the matchups of in situ and MULTIOBS data points in the 0–20 and 20–60 m depth layers is very strong and significant (r $\geq$ 0.88, *p* < 0.001) (Figure 5a,c), and the distributions of the matched in situ and MULTIOBS data at the E1-M3A site are quite similar in terms of the range of values and mostly overlap (Figure 5b,d). However, the RMSE suggests an almost 1.6- and 1.3-fold deviation, on average, between MULTIOBS and in situ data within the 0–20 m and 20–60 m depth layers, respectively. There is a slight overestimation by the MULTIOBS product within the upper surface layer (0–20 m) at the level of 29% (Figure 5a). Conversely, the product has an excellent performance in terms of accuracy within the 20–60 m layer, as shown by the minuscule bias (5% underestimation) estimated for this layer (Figure 5c). The comparison of climatologies computed for the MULTIOBS and in situ data reveals that within the surface layer, the observed overestimation is mostly evident during the stratified season (Figure S7a), whereas for the 20–60 m depth layer, the underestimation is mostly evident during the bloom–intermediate (January–April) period (Figure S7b). Nevertheless, the overall good agreement between the climatologies computed for the MULTIOBS and in situ data suggests a high competency of MULTIOBS to capture the seasonal signal and reproduce the annual maxima and minima of the time series. Finally, MULTIOBS adequately reproduces the interannual variability, as is evident by the significant positive correlation (r $\geq$ 0.55, *p* < 0.001) of monthly standardised anomalies of in situ and MULTIOBS matchups within the 0–20 m and 20–60 m layers (Figure S8a,b).

The correlation between MULTIOBS and in situ is lower, albeit significant, within the deeper layers (60–100 m, r = 0.44, *p* = 0.002; and 100–120 m, r = 0.59, *p* < 0.001) (Figure 5e,g). The RMSE suggests a 1.4-fold average deviation from in situ data for the 60–100 m layer (Figure 5e) and up to 1.6-fold average deviation for the 100–120 m layer (Figure 5g). However, the bias suggests a low level of Chl-a underestimation by the MULTIOBS product at ~15% in both layers. Especially within the 60–100 m layer, where the DCM is located (Figures 2 and 4a), the interannual variability can be quite significant, as is evident from the in situ time series at the E1-M3A site (Figure 5e), where the data appear distributed quite randomly, both at seasonal and interannual time scales. The distribution of the matched in situ data suggests a wide range of in situ Chl-a concentrations, whereas the corresponding

estimates from the MULTIOBS product have a rather different distribution being tightly aggregated around the distribution's mean with a smaller range of possible Chl-a values (Figure 5f). An explanation of the loss of the correlation strength could be the vertical resolution of the MULTIOBS product, which becomes coarser, providing a measurement every 10 m within the 70–100 m layer, as opposed to the 5 m resolution within the 0–70 m layer, resulting in smoother profile shapes as compared with the in situ ones (Figure 2). This could potentially be a limitation during the period when DCM is present in the EMS. During this period, in situ profiles rarely follow this smooth shape, and they often exhibit local peaks with variable width, as is evident from the variability in the climatological profiles in Figure 2. This variability could be due to the interplay of various physical and biological factors (vertical mixing, grazing, light and nutrient availability) [53], as well as due to the diversity in vertical distributions of the phytoplankton taxa occupying this layer [73]. Our results suggest that future releases of the product should aim to provide a higher resolution within this ecologically important layer to capture its fine-scale variability. The correlation coefficient increases slightly within the deepest layer (100–120 m) of our dataset (Figure 5g), while the distributions of matched MULTIOBS and in situ data show a better agreement (Figure 5h) as compared with the overlaying layer (Figure 5e,f), suggesting a slight improvement in the ability of MULTIOBS to capture the Chl-a dynamics, despite the even coarser resolution (25 m). The increase in the correlation strength between in situ and MULTIOBS data likely reflects a transition from the biologically active 60–100 m layer, where the DCM occurs and multiple ecological processes influence phytoplankton biomass accumulation, to the deeper (100–120 m), less dynamic layer. This deeper layer exhibits a more stable seasonal cycle and lower interannual fluctuations, facilitating the representation of in situ variability by the MULTIOBS machine learning algorithm. Nevertheless, the 100–120 m layer would also be affected, albeit to a lower extent, by the biogeochemical and physical processes shaping the above DCM layer, particularly during the late stratification period (July–September) when the DCM is often located around 100 m or extends deeper on certain occasions. These processes likely influence Chl-a in the 100–120 m layer and help explain why MULTIOBS performs less effectively in capturing in situ variability in this depth range compared with the surface layers (0–60 m). Finally, the product appears very consistent with the in situ data at certain occasions, such as during 2013–2014.

The comparison of the mean annual cycle computed for the matchups between MULTIOBS and in situ data suggests that the product adequately captures the seasonal signal and reproduces the annual maxima and minima of the time series within the deeper layers, a finding that signifies the ability of the MULTIOBS to capture Chl-a redistribution throughout the water column over the seasonal cycle (Figure S7c,d). However, a substantial underestimation in both the 60–100 and 100–120 m layers is observed. Moreover, the product fails to reproduce the interannual variability of in situ data, as evidenced by the absence of significant correlation of monthly standardised anomalies of in situ and MULTIOBS matchups within the deeper layers of the water column (Figure S8c,d). Nevertheless, the covariation of anomalies suggests that the product can be used to capture positive and negative anomalies in Chl-a concentration within the deeper layers of the EMS euphotic zone.

When considering the whole water column (0–120 m), the correlation between the MULTIOBS product and the in situ data is significant (r = 0.64, $p < 0.001$), and the product reproduces the interannual variability in the annual maxima in most cases (Figure 6). Thus, the partial inconsistencies mostly observed within the 60–100 m layer do not seem to have a significant impact on the bulk Chl-a within the 0–120 m layer. The product underestimates the bulk Chl-a within the 0–120 m by only 9%, and the RMSE suggests a 1.3-fold average deviation between MULTIOBS and in situ values. By comparing the climatologies for the matchups between MULTIOBS and in situ data, it becomes evident that the product adequately reproduces the seasonality of in situ data by capturing the timing of Chl-a maximum and minimum for the 0–120 m layer (Figure S9a). However, the observed underestimation of Chl-a is mostly evident during the productive–early stratified period (January–May). Finally, the positive and significant correlation of Chl-a anomalies

computed for in situ and MULTIOBS matchups (r = 0.34, *p* = 0.032) suggests an adequate performance of the product in reproducing interannual variability as it can capture positive and negative anomalies in Chl-a within the euphotic zone of the EMS, although discrepancies may occur in terms of the absolute values of these anomalies (Figure S9b). It is important to acknowledge that the limited availability of in situ profiles presents an important challenge in evaluating MULTIOBS's capacity to capture interannual variability. Nevertheless, the product's performance remains satisfactory despite these constraints. Importantly, the integrated Chl-a over the 0–120 m zone provides a good representation of phytoplankton abundance in the water column. This enables the investigation of interannual variability in ecological indicators (e.g., phenology) and their link with higher trophic levels [74], under the influence of a warming Mediterranean Sea.

4. Conclusions

MULTIOBS provides vertical profiles of Chl-a on a regular spatial grid (0.25° × 0.25°) and on a weekly temporal resolution, globally. Due to its 3D architecture, it offers a unique opportunity for studying Chl-a dynamics throughout the water column with unprecedented spatial and temporal resolution, eventually paving the way for a more accurate assessment of marine ecosystems productivity across the entire productive zone. The present study provides an independent evaluation of MULTIOBS Chl-a product, focusing specifically on the ultra-oligotrophic EMS, and represents a first step towards the application of this product for studying phytoplankton dynamics in oligotrophic systems.

The MULTIOBS product was able to capture the seasonal evolution of the Chl-a vertical distribution in the EMS in response to vertical mixing and stratification in the water column. The depth of the Chl-a maximum and its seasonal migration along the vertical axis is also adequately represented by the product. The ability of MULTIOBS to accurately capture seasonal and interannual variability at the E1-M3A site, a fixed monitoring station in the EMS, was also evaluated. The results from this analysis are promising, indicating that MULTIOBS performs well in reflecting year-to-year changes observed at the site. Despite the overall good performance of MULTIOBS in reproducing Chl-a vertical profiles, some discrepancies were observed compared with in situ Chl-a values, particularly at the lower and upper ends of the Chl-a range. Chl-a values >0.3 mg m^{-3} can be encountered during the blooming period in the EMS or in the vicinity of the DCM layer during the stratified season. In these cases, the MULTIOBS product tends to slightly underestimate Chl-a. On the other hand, very low Chl-a values (0.01–0.05 mg m^{-3}), typically found in the surface layer of the EMS during the stratified season, were slightly overestimated by MULTIOBS. Nevertheless, as more Chl-a vertical profiles become available and are incorporated into the machine learning algorithm of the MULTIOBS product, allowing for a more representative training dataset reflecting the entire range of Chl-a that can be encountered in the EMS, these discrepancies are expected to lower. Additionally, the Argo Data Management Team [75] is committed to continuously enhancing the accuracy of Argo data and improving the Chl-a estimates derived from in situ fluorometers on board BGC-Argo floats, aiming for increasingly reliable results in the future. Increasing the spatiotemporal resolution of MULTIOBS as well as its depth resolution, especially within the deeper layers (>70 m), is also expected to improve the product's performance in capturing fine-scale variability of Chl-a in the horizontal and vertical dimensions.

Overall, our assessment suggests that the MULTIOBS product is a valuable tool for conducting in-depth analyses of phytoplankton dynamics throughout the entire euphotic zone. Two main traits of this product make it extremely useful for disentangling the effects of environmental perturbations, such as oceanic warming, on phytoplankton dynamics. First, it conveys information for phytoplankton across the vertical dimension unlike satellite-derived data, which only represents the ocean's surface layer. Second, it offers continuous spatial and temporal coverage, unlike the data obtained via BGC-Argo profile floats, making MULTIOBS an ideal tool for describing the long-term spatiotemporal variability of phytoplankton within the poorly understood subsurface layer of the ocean. The MULTIOBS

product opens new avenues for research into phytoplankton dynamics and phenology, both in terms of biomass and vertical distribution, in response to oceanic warming. Moreover, the MULTIOBS data could be used to better understand the relationship between Chl-a and phytoplankton carbon along the vertical dimension, considering the b_{bp} and POC data also available through the MULTIOBS product. This may result in optimised estimates of vertically resolved primary productivity, leading to a more comprehensive understanding of the contribution of subsurface layers to carbon flux and export at depth and higher trophic levels.

Supplementary Materials: The following supporting information can be downloaded at: https://www.mdpi.com/article/10.3390/rs16244705/s1, Figure S1: Examples of non-photochemical quenching (NPQ)-corrected and -uncorrected fluorescence-derived profiles and HPLC-derived, corrected for NPQ and calibrated final profiles at two contrasting seasons; Figure S2: Examples of non-photochemical quenching (NPQ)-corrected and -uncorrected fluorescence-derived profiles and HPLC-derived, uncorrected for NPQ and calibrated final Chl-a profiles at two contrasting seasons; Figure S3: Mean absolute difference between MULTIOBS and in situ Chl-a per month; Figure S4: Scatterplots of the relative residuals of the matchups between in situ- and MULTIOBS-derived Chl-a over the Eastern Mediterranean Sea vs in situ Chl-a; Figure S5: Histograms of the relative residuals of the matchups between in situ- and MULTIOBS-derived Chl-a over the Eastern Mediterranean Sea; Figure S6: Scatterplots of the matchups between in situ HPLC-evaluated Chl-a bottle data and MULTIOBS-derived Chl-a over the Eastern Mediterranean Sea; Figure S7: Monthly averaged Chl-a for the E1-M3A site at the Eastern Mediterranean Sea (north of Crete) derived from the in situ data and the corresponding matched monthly averaged Chl-a data obtained from the MULTIOBS product presented as mean integrals of successive depth layers; Figure S8: Scatterplots of standardised monthly anomalies of the matched, for the E1-M3A site at the Eastern Mediterranean Sea (north of Crete), in situ- and MULTIOBS-derived Chl-a mean integrals of successive depth layers; Figure S9: (a) Monthly averaged Chl-a for the E1-M3A site at the Eastern Mediterranean Sea (north of Crete) derived from the in situ data and the corresponding matched monthly averaged Chl-a data obtained from the MULTIOBS product presented as mean integrals of the 0–120 m layer, (b) Scatterplot of standardised monthly anomalies for the matched in situ- and MULTIOBS-derived Chl-a mean integrals of the 0–120 m layer for the E1-M3A site at the Eastern Mediterranean Sea (north of Crete).

References

1. Pastor, F.; Valiente, J.A.; Khodayar, S. A Warming Mediterranean: 38 Years of Increasing Sea Surface Temperature. *Remote Sens.* **2020**, *12*, 2687. [CrossRef]
2. Raitsos, D.E.; Beaugrand, G.; Georgopoulos, D.; Zenetos, A.; Pancucci-Papadopoulou, A.M.; Theocharis, A.; Papathanassiou, E. Global Climate Change Amplifies the Entry of Tropical Species into the Eastern Mediterranean Sea. *Limnol. Oceanogr.* **2010**, *55*, 1478–1484. [CrossRef]
3. Giorgi, F. Climate Change Hot-spots. *Geophys. Res. Lett.* **2006**, *33*, L08707. [CrossRef]
4. Zittis, G.; Almazroui, M.; Alpert, P.; Ciais, P.; Cramer, W.; Dahdal, Y.; Fnais, M.; Francis, D.; Hadjinicolaou, P.; Howari, F.; et al. Climate Change and Weather Extremes in the Eastern Mediterranean and Middle East. *Rev. Geophys.* **2022**, *60*, e2021RG000762. [CrossRef]
5. Bethoux, J.P.; Gentili, B.; Morin, P.; Nicolas, E.; Pierre, C.; Ruiz-Pino, D. The Mediterranean Sea: A Miniature Ocean for Climatic and Environmental Studies and a Key for the Climatic Functioning of the North Atlantic. *Prog. Oceanogr.* **1999**, *44*, 131–146. [CrossRef]
6. Lejeusne, C.; Chevaldonné, P.; Pergent-Martini, C.; Boudouresque, C.F.; Pérez, T. Climate Change Effects on a Miniature Ocean: The Highly Diverse, Highly Impacted Mediterranean Sea. *Trends Ecol. Evol.* **2010**, *25*, 250–260. [CrossRef] [PubMed]
7. Morel, A.; Berthon, J. Surface Pigments, Algal Biomass Profiles, and Potential Production of the Euphotic Layer: Relationships Reinvestigated in View of Remote-sensing Applications. *Limnol. Oceanogr.* **1989**, *34*, 1545–1562. [CrossRef]
8. Psarra, S.; Tselepides, A.; Ignatiades, L. Primary Productivity in the Oligotrophic Cretan Sea (NE Mediterranean): Seasonal and Interannual Variability. *Prog. Oceanogr.* **2000**, *46*, 187–204. [CrossRef]
9. Reich, T.; Ben-Ezra, T.; Belkin, N.; Tsemel, A.; Aharonovich, D.; Roth-Rosenberg, D.; Givati, S.; Bialik, M.; Herut, B.; Berman-Frank, I.; et al. A Year in the Life of the Eastern Mediterranean: Monthly Dynamics of Phytoplankton and Bacterioplankton in an Ultra-Oligotrophic Sea. *Deep Sea Res. Part I Oceanogr. Res. Pap.* **2022**, *182*, 103720. [CrossRef]
10. Moutin, T.; Raimbault, P. Primary Production, Carbon Export and Nutrients Availability in Western and Eastern Mediterranean Sea in Early Summer 1996 (MINOS Cruise). *J. Mar. Syst.* **2002**, *33–34*, 273–288. [CrossRef]
11. Varkitzi, I.; Psarra, S.; Assimakopoulou, G.; Pavlidou, A.; Krasakopoulou, E.; Velaoras, D.; Papathanassiou, E.; Pagou, K. Phytoplankton Dynamics and Bloom Formation in the Oligotrophic Eastern Mediterranean: Field Studies in the Aegean, Levantine and Ionian Seas. *Deep Sea Res. Part II Top. Stud. Oceanogr.* **2020**, *171*, 104662. [CrossRef]
12. Barbieux, M.; Uitz, J.; Gentili, B.; Pasqueron de Fommervault, O.; Mignot, A.; Poteau, A.; Schmechtig, C.; Taillandier, V.; Leymarie, E.; Penkerc'h, C.; et al. Bio-Optical Characterization of Subsurface Chlorophyll Maxima in the Mediterranean Sea from a Biogeochemical-Argo Float Database. *Biogeosciences* **2019**, *16*, 1321–1342. [CrossRef]
13. D'Ortenzio, F.; Taillandier, V.; Claustre, H.; Coppola, L.; Conan, P.; Dumas, F.; Durrieu Du Madron, X.; Fourrier, M.; Gogou, A.; Karageorgis, A.; et al. BGC-Argo Floats Observe Nitrate Injection and Spring Phytoplankton Increase in the Surface Layer of Levantine Sea (Eastern Mediterranean). *Geophys. Res. Lett.* **2021**, *48*, e2020GL091649. [CrossRef]
14. Mignot, A.; Claustre, H.; Uitz, J.; Poteau, A.; D'Ortenzio, F.; Xing, X. Understanding the Seasonal Dynamics of Phytoplankton Biomass and the Deep Chlorophyll Maximum in Oligotrophic Environments: A Bio-Argo Float Investigation. *Glob. Biogeochem. Cycles* **2014**, *28*, 856–876. [CrossRef]
15. Lazzari, P.; Solidoro, C.; Ibello, V.; Salon, S.; Teruzzi, A.; Béranger, K.; Colella, S.; Crise, A. Seasonal and Inter-Annual Variability of Plankton Chlorophyll and Primary Production in the Mediterranean Sea: A Modelling Approach. *Biogeosciences* **2012**, *9*, 217–233. [CrossRef]
16. Macías, D.; Stips, A.; Garcia-Gorriz, E. The Relevance of Deep Chlorophyll Maximum in the Open Mediterranean Sea Evaluated through 3D Hydrodynamic-Biogeochemical Coupled Simulations. *Ecol. Model.* **2014**, *281*, 26–37. [CrossRef]
17. Lavigne, H.; D'Ortenzio, F.; Ribera D'Alcalà, M.; Claustre, H.; Sauzède, R.; Gacic, M. On the Vertical Distribution of the Chlorophyll a Concentration in the Mediterranean Sea: A Basin-Scale and Seasonal Approach. *Biogeosciences* **2015**, *12*, 5021–5039. [CrossRef]
18. Siokou-Frangou, I.; Christaki, U.; Mazzocchi, M.G.; Montresor, M.; Ribera d'Alcalá, M.; Vaqué, D.; Zingone, A. Plankton in the Open Mediterranean Sea: A Review. *Biogeosciences* **2010**, *7*, 1543–1586. [CrossRef]
19. Petihakis, G.; Perivoliotis, L.; Korres, G.; Ballas, D.; Frangoulis, C.; Pagonis, P.; Ntoumas, M.; Pettas, M.; Chalkiopoulos, A.; Sotiropoulou, M.; et al. An Integrated Open-Coastal Biogeochemistry, Ecosystem and Biodiversity Observatory of the Eastern Mediterranean—The Cretan Sea Component of the POSEIDON System. *Ocean Sci.* **2018**, *14*, 1223–1245. [CrossRef]
20. Sauzède, R.; Renosh, P.R.; Schmechtig, C.; Uitz, J.; Claustre, H. Quality Information Document. Global Ocean 3D Particulate Organic Carbon and Chlorophyll-a Concentration Product MULTIOBS_GLO_BIO_BGC_3D_REP_015_010. 2024. Available online: https://catalogue.marine.copernicus.eu/documents/QUID/CMEMS-MOB-QUID-015-010.pdf (accessed on 11 December 2024).
21. Global Ocean 3D Chlorophyll-a Concentration, Particulate Backscattering Coefficient and Particulate Organic Carbon; E.U. Copernicus Marine Service Information (CMEMS). Marine Data Store (MDS). Available online: https://data.marine.copernicus.eu/product/MULTIOBS_GLO_BIO_BGC_3D_REP_015_010/description (accessed on 11 December 2024). [CrossRef]
22. Sauzède, R.; Claustre, H.; Uitz, J.; Jamet, C.; Dall'Olmo, G.; D'Ortenzio, F.; Gentili, B.; Poteau, A.; Schmechtig, C. A Neural Network-based Method for Merging Ocean Color and Argo Data to Extend Surface Bio-optical Properties to Depth: Retrieval of the Particulate Backscattering Coefficient. *JGR Ocean.* **2016**, *121*, 2552–2571. [CrossRef]

23. Claustre, H.; Johnson, K.S.; Takeshita, Y. Observing the Global Ocean with Biogeochemical-Argo. *Annu. Rev. Mar. Sci.* **2020**, *12*, 23–48. [CrossRef] [PubMed]

24. Multi Observation Global Ocean 3D Temperature Salinity Height Geostrophic Current and MLD; E.U. Copernicus Marine Service Information (CMEMS), Marine Data Store (MDS). Available online: https://data.marine.copernicus.eu/product/MULTIOBS_GLO_PHY_TSUV_3D_MYNRT_015_012/description (accessed on 11 December 2024). [CrossRef]

25. Global Ocean Colour (Copernicus-GlobColour), Bio-Geo-Chemical, L3 (Daily) from Satellite Observations (1997-Ongoing); E.U. Copernicus Marine Service Information (CMEMS), Marine Data Store (MDS). Available online: https://data.marine.copernicus.eu/product/OCEANCOLOUR_GLO_BGC_L3_MY_009_103/description (accessed on 11 December 2024). [CrossRef]

26. Global Ocean Gridded L 4 Sea Surface Heights and Derived Variables Reprocessed 1993 Ongoing. E.U. Copernicus Marine Service Information (CMEMS). Marine Data Store (MDS). Available online: https://data.marine.copernicus.eu/product/SEALEVEL_GLO_PHY_L4_MY_008_047/description (accessed on 11 December 2024). [CrossRef]

27. GlobColour Data. Available online: https://hermes.acri.fr/?class=archive (accessed on 11 September 2024).

28. Lagaria, A.; Mandalakis, M.; Mara, P.; Frangoulis, C.; Karatsolis, B.-T.; Pitta, P.; Triantaphyllou, M.; Tsiola, A.; Psarra, S. Phytoplankton Variability and Community Structure in Relation to Hydrographic Features in the NE Aegean Frontal Area (NE Mediterranean Sea). *Cont. Shelf Res.* **2017**, *149*, 124–137. [CrossRef]

29. Taillandier, V.; Wagener, T.; D'Ortenzio, F.; Mayot, N.; Legoff, H.; Ras, J.; Coppola, L.; Pasqueron De Fommervault, O.; Schmechtig, C.; DIamond, E.; et al. Hydrography and Biogeochemistry Dedicated to the Mediterranean BGC-Argo Network during a Cruise with RV Tethys 2 in May 2015. *Earth Syst. Sci. Data* **2018**, *10*, 627–641. [CrossRef]

30. D'Ortenzio, F.; Thierry, V.; Eldin, G.; Claustre, H.; Testor, P.; Coatanoan, C.; Tedetti, M.; Guinet, C.; Poteau, A.; Prieur, L.; et al. White Book on Oceanic Autonomous Platforms for Biogeochemical Studies: Instrumentation and Measure (PABIM) Version 1.3. 2010. Available online: https://www.coriolis.eu.org/News-Events/Latest-News/PABIM-White-BOOK (accessed on 5 November 2023).

31. Xing, X.; Claustre, H.; Blain, S.; D'Ortenzio, F.; Antoine, D.; Ras, J.; Guinet, C. Quenching Correction for In Vivo Chlorophyll Fluorescence Acquired by Autonomous Platforms: A Case Study with Instrumented Elephant Seals in the Kerguelen Region (Southern Ocean). *Limnol. Oceanogr. Methods* **2012**, *10*, 483–495. [CrossRef]

32. de Boyer Montégut, C.; Madec, G.; Fischer, A.S.; Lazar, A.; Iudicone, D. Mixed Layer Depth over the Global Ocean: An Examination of Profile Data and a Profile-Based Climatology. *J. Geophys. Res. Ocean.* **2004**, *109*, C12003. [CrossRef]

33. Roesler, C.; Uitz, J.; Claustre, H.; Boss, E.; Xing, X.; Organelli, E.; Briggs, N.; Bricaud, A.; Schmechtig, C.; Poteau, A.; et al. Recommendations for Obtaining Unbiased Chlorophyll Estimates from in Situ Chlorophyll Fluorometers: A Global Analysis of WET Labs ECO Sensors. *Limnol. Oceanogr. Methods* **2017**, *15*, 572–585. [CrossRef]

34. Petit, F.; Uitz, J.; Schmechtig, C.; Dimier, C.; Ras, J.; Poteau, A.; Golbol, M.; Vellucci, V.; Claustre, H. Influence of the Phytoplankton Community Composition on the In Situ Fluorescence Signal: Implication for an Improved Estimation of the Chlorophyll-a Concentration from BioGeoChemical-Argo Profiling Floats. *Front. Mar. Sci.* **2022**, *9*, 959131. [CrossRef]

35. Brewin, R.J.W.; Raitsos, D.E.; Pradhan, Y.; Hoteit, I. Comparison of Chlorophyll in the Red Sea Derived from MODIS-Aqua and in Vivo Fluorescence. *Remote Sens. Environ.* **2013**, *136*, 218–224. [CrossRef]

36. Seegers, B.N.; Stumpf, R.P.; Schaeffer, B.A.; Loftin, K.A.; Werdell, P.J. Performance Metrics for the Assessment of Satellite Data Products: An Ocean Color Case Study. *Opt. Express* **2018**, *26*, 7404. [CrossRef]

37. Virtanen, P.; Gommers, R.; Oliphant, T.E.; Haberland, M.; Reddy, T.; Cournapeau, D.; Burovski, E.; Peterson, P.; Weckesser, W.; Bright, J.; et al. SciPy 1.0: Fundamental Algorithms for Scientific Computing in Python. *Nat. Methods* **2020**, *17*, 261–272. [CrossRef] [PubMed]

38. Seabold, S.; Perktold, J. Statsmodels: Econometric and Statistical Modeling with Python. In Proceedings of the 9th Python in Science Conference, Austin, TX, USA, 28 June–3 July 2010. [CrossRef]

39. Waskom, M.L. Seaborn: Statistical Data Visualization. *J. Open Source Softw.* **2021**, *6*, 3021. [CrossRef]

40. McKinney, W. Data Structures for Statistical Computing in Python. In Proceedings of the 9th Python in Science Conference, Austin, TX, USA, 28 June–3 July 2010; pp. 56–61. [CrossRef]

41. Hoyer, S.; Hammer, J. Xarray: N-D Labeled Arrays and Datasets in Python. *J. Open Res. Softw.* **2017**, *5*, 10. [CrossRef]

42. Hunter, J.D. Matplotlib: A 2D Graphics Environment. *Comput. Sci. Eng.* **2007**, *9*, 90–95. [CrossRef]

43. Met Office Cartopy: A Cartographic Python Library with a Matplotlib Interface. Available online: https://scitools.org.uk/cartopy (accessed on 5 November 2023).

44. D'Ortenzio, F.; Ribera d'Alcalà, M. On the Trophic Regimes of the Mediterranean Sea: A Satellite Analysis. *Biogeosciences* **2009**, *6*, 139–148. [CrossRef]

45. Lavigne, H.; D'Ortenzio, F.; Migon, C.; Claustre, H.; Testor, P.; d'Alcalà, M.R.; Lavezza, R.; Houpert, L.; Prieur, L. Enhancing the Comprehension of Mixed Layer Depth Control on the Mediterranean Phytoplankton Phenology: Mediterranean Phytoplankton Phenology. *J. Geophys. Res. Ocean.* **2013**, *118*, 3416–3430. [CrossRef]

46. Malanotte-Rizzoli, P.; Artale, V.; Borzelli-Eusebi, G.L.; Brenner, S.; Crise, A.; Gacic, M.; Kress, N.; Marullo, S.; Ribera d'Alcalà, M.; Sofianos, S.; et al. Physical Forcing and Physical/Biochemical Variability of the Mediterranean Sea: A Review of Unresolved Issues and Directions for Future Research. *Ocean Sci.* **2014**, *10*, 281–322. [CrossRef]

47. Theocharis, A.; Balopoulos, E.; Kioroglou, S.; Kontoyiannis, H.; Iona, A. A Synthesis of the Circulation and Hydrography of the South Aegean Sea and the Straits of the Cretan Arc (March 1994–January 1995). *Progr. Oceanogr.* **1999**, *44*, 469–509. [CrossRef]

48. McGillicuddy, D.J. Mechanisms of Physical-Biological-Biogeochemical Interaction at the Oceanic Mesoscale. *Annu. Rev. Mar. Sci.* **2016**, *8*, 125–159. [CrossRef] [PubMed]

49. Müller, P.; Li, X.-P.; Niyogi, K.K. Non-Photochemical Quenching. A Response to Excess Light Energy. *Plant Physiol.* **2001**, *125*, 1558–1566. [CrossRef] [PubMed]

50. Terrats, L.; Claustre, H.; Cornec, M.; Mangin, A.; Neukermans, G. Detection of Coccolithophore Blooms With BioGeoChemical-Argo Floats. *Geophys. Res. Lett.* **2020**, *47*, e2020GL090559. [CrossRef]

51. Xing, X.; Briggs, N.; Boss, E.; Claustre, H. Improved Correction for Non-Photochemical Quenching of in Situ Chlorophyll Fluorescence Based on a Synchronous Irradiance Profile. *Opt. Express* **2018**, *26*, 24734. [CrossRef] [PubMed]

52. Schmechtig, C.; Claustre, H.; Poteau, A.; D'Ortenzio, F.; Schallenberg, C.; Trull, T.; Xing, X. BGC-Argo Quality Control Manual for the Chlorophyll-A Concentration; Ifremer. 2023. Available online: https://archimer.ifremer.fr/doc/00243/35385/ (accessed on 11 September 2024). [CrossRef]

53. Cullen, J.J. Subsurface Chlorophyll Maximum Layers: Enduring Enigma or Mystery Solved? *Annu. Rev. Mar. Sci.* **2015**, *7*, 19.1–19.33. [CrossRef]

54. Estrada, M.; Marrasé, C.; Latasa, M.; Berdalet, E.; Delgado, M.; Riera, T. Variability of Deep Chlorophyll Maximum Characteristics in the Northwestern Mediterranean. *Mar. Ecol. Prog. Ser.* **1993**, *92*, 289–300. [CrossRef]

55. Marañón, E.; Van Wambeke, F.; Uitz, J.; Boss, E.; Pérez-Lorenzo, M.; Dinasquet, J.; Haëntjens, N.; Dimier, C.; Taillandier, V. Deep Maxima of Phytoplankton Biomass, Primary Production and Bacterial Production in the Mediterranean Sea during Late Spring. *Biogeosciences* **2021**, *18*, 1749–1767. [CrossRef]

56. Cornec, M.; Claustre, H.; Mignot, A.; Guidi, L.; Lacour, L.; Poteau, A.; D'Ortenzio, F.; Gentili, B.; Schmechtig, C. Deep Chlorophyll Maxima in the Global Ocean: Occurrences, Drivers and Characteristics. *Glob. Biogeochem. Cycles* **2021**, *35*, e2020GB006759. [CrossRef]

57. Geider, R.; MacIntyre, H.; Kana, T. Dynamic Model of Phytoplankton Growth and Acclimation: Responses of the Balanced Growth Rate and the Chlorophyll a: Carbon Ratio to Light, Nutrient-Limitation and Temperature. *Mar. Ecol. Prog. Ser.* **1997**, *148*, 187–200. [CrossRef]

58. Kiefer, D.A.; Olson, R.J.; Holm-Hansen, O. Another Look at the Nitrite and Chlorophyll Maxima in the Central North Pacific. *Deep. Sea Res. Oceanogr. Abstr.* **1976**, *23*, 1199–1208. [CrossRef]

59. Steele, J.H. A Study of Production in the Gulf of Mexico. *J. Mar. Res.* **1964**, *22*, 211–222.

60. Bouman, H.A.; Jackson, T.; Sathyendranath, S.; Platt, T. Vertical Structure in Chlorophyll Profiles: Influence on Primary Production in the Arctic Ocean. *Philos. Trans. R. Soc. A* **2020**, *378*, 20190351. [CrossRef]

61. Platt, T.; Sathyendranath, S.; Caverhill, C.M.; Lewis, M.R. Ocean Primary Production and Available Light: Further Algorithms for Remote Sensing. *Deep Sea Res. Part I Oceanogr. Res. Pap.* **1988**, *35*, 855–879. [CrossRef]

62. Platt, T.; Sathyendranath, S. Oceanic Primary Production: Estimation by Remote Sensing at Local and Regional Scales. *Science* **1988**, *241*, 1613–1620. [CrossRef]

63. Mignot, A.; Claustre, H.; D'Ortenzio, F.; Xing, X.; Poteau, A.; Ras, J. From the Shape of the Vertical Profile of In Vivo Fluorescence to Chlorophyll-a Concentration. *Biogeosciences* **2011**, *8*, 2391–2406. [CrossRef]

64. Brewin, R.J.W.; Dall'Olmo, G.; Gittings, J.; Sun, X.; Lange, P.K.; Raitsos, D.E.; Bouman, H.A.; Hoteit, I.; Aiken, J.; Sathyendranath, S. A Conceptual Approach to Partitioning a Vertical Profile of Phytoplankton Biomass into Contributions from Two Communities. *JGR Ocean.* **2022**, *127*, e2021JC018195. [CrossRef] [PubMed]

65. Benway, H.M.; Lorenzoni, L.; White, A.E.; Fiedler, B.; Levine, N.M.; Nicholson, D.P.; DeGrandpre, M.D.; Sosik, H.M.; Church, M.J.; O'Brien, T.D.; et al. Ocean Time Series Observations of Changing Marine Ecosystems: An Era of Integration, Synthesis, and Societal Applications. *Front. Mar. Sci.* **2019**, *6*, 393. [CrossRef]

66. Platt, T.; Sathyendranath, S. Ecological Indicators for the Pelagic Zone of the Ocean from Remote Sensing. *Remote Sens. Environ.* **2008**, *112*, 3426–3436. [CrossRef]

67. Behrenfeld, M.J.; O'Malley, R.T.; Boss, E.S.; Westberry, T.K.; Graff, J.R.; Halsey, K.H.; Milligan, A.J.; Siegel, D.A.; Brown, M.B. Revaluating Ocean Warming Impacts on Global Phytoplankton. *Nat. Clim. Chang.* **2016**, *6*, 323–330. [CrossRef]

68. Raitsos, D.E.; Yi, X.; Platt, T.; Racault, M.; Brewin, R.J.W.; Pradhan, Y.; Papadopoulos, V.P.; Sathyendranath, S.; Hoteit, I. Monsoon Oscillations Regulate Fertility of the Red Sea. *Geophys. Res. Lett.* **2015**, *42*, 855–862. [CrossRef]

69. Noh, K.M.; Lim, H.-G.; Kug, J.-S. Global Chlorophyll Responses to Marine Heatwaves in Satellite Ocean Color. *Environ. Res. Lett.* **2022**, *17*, 064034. [CrossRef]

70. Tang, W.; Llort, J.; Weis, J.; Basart, S.; Li, Z.; Sathyendranath, S.; Jackson, T.; Perron, M.; Sanz Rodriguez, E.; Proemse, B.; et al. Widespread Phytoplankton Blooms Triggered by 2019-2020 Australian Wildfires. *Nature* **2021**, *597*, 370–375. [CrossRef]

71. Cole, H.; Henson, S.; Martin, A.; Yool, A. Mind the Gap: The Impact of Missing Data on the Calculation of Phytoplankton Phenology Metrics. *J. Geophys. Res.* **2012**, *117*, C08030. [CrossRef]

72. Racault, M.-F.; Sathyendranath, S.; Platt, T. Impact of Missing Data on the Estimation of Ecological Indicators from Satellite Ocean-Colour Time-Series. *Remote Sens. Environ.* **2014**, *152*, 15–28. [CrossRef]

73. Latasa, M.; Cabello, A.M.; Morán, X.A.G.; Massana, R.; Scharek, R. Distribution of Phytoplankton Groups Within the Deep Chlorophyll Maximum: Distribution of Phytoplankton Groups in the DCM. *Limnol. Oceanogr.* **2017**, *62*, 665–685. [CrossRef]

74. Platt, T.; Fuentes-Yaco, C.; Frank, T.H. Spring Algal Bloom and Larval Fish Survival. *Nature* **2003**, *423*, 398–399. [CrossRef] [PubMed]

75. Argo. Argo Float Data and Metadata from Global Data Assembly Centre (Argo GDAC). SEANOE. 2024. Available online: https://www.seanoe.org/data/00311/42182/ (accessed on 11 September 2024). [CrossRef]